# Effect of the nanopores in the $Al_-Cu$ intermetallic phase on nanoindentation instabilities at the Al/Cu interface of a magnetic pulse impact weld

R.N. Raoelison[1,2]*, J. Li[2,3], T. Sapanathan[2,3,4], A. Favache[3], A. Simar[3], M. Rachik[2]

[1] Université de Technologie de Belfort-Montbéliard, CNRS, ICB, F-90010 Belfort cedex, France

[2] Sorbonne universités, Université de technologie de Compiègne, laboratoire Roberval, FRE 2012 CNRS, Centre de recherche Royallieu, CS 60319, 60203 Compiègne cedex, France

[3] Université catholique de Louvain, Institute of Mechanics, Materials and Civil Engineering, Louvain-la-Neuve, Belgium

[4] Curtin Corrosion Centre, WA School of Mines: Minerals, Energy and Chemical Engineering, Faculty of Science and Engineering, Curtin University, Perth Australia

Corresponding author: rija-nirina.raoelison@utbm.fr, jishuai.li@outlook.com

## Abstract

This paper investigates the features of an $Al_xCu_y$ intermetallic phase produced by the high strain rate collision at an Al/Cu interface during magnetic pulse impact welding. A SEM observation coupled with a EDX analysis reveals a nanoporous $Al_2Cu$ phase. A mechanical characterization using a high resolution nanoindentation shows a P-h curve with a pop-in phenomenon which is attributed to the nanoporosity of the $Al_2Cu$ phase. As the nanoporosity fraction increases from ~1 % to ~6 %, the hardness decreases twofold with a linear tendency. The total cumulative length of pop-ins increases with the nanopores fraction, with a linear tendency also. The critical force of pop-ins is lowered by the porosity content. The curve of highest porosity fraction exhibits the lowest values of critical force. These observations correlate the nanopores to the pop-ins. Compared to the parent metals, the $Al_2Cu$ intermetallic phase exhibits a higher hardness in between 4-10 GPa.

**Keywords:** magnetic pulse impact welding, intermetallics, nanoporous, hardness, pop-ins1.

## 1. Introduction

High speed impact welding is an innovative joining process with a capability to weld dissimilar alloys for diverse metals combinations across a broad range of structure scale [1]. This welding principle falls into four major techniques [2], that are, explosive welding (EXW), water jet welding (WJW), laser spot welding or laser shock welding (LSW), magnetic pulse welding (MPW) and vaporizing foil actuator welding (VFAW) [1,3–5]. During the high-speed collision, the interface is subjected to multiscale complex phenomena at different scales. At the macroscopic scale of the interface, there is the well-known kinematic instability that leads to the formation of diverse morphologies (wavy interface, regularly or irregularly shaped interface, jetting, vortex occurrence), explained as a result of a cascade of instabilities [6,7]. At finer scales, there is the formation of submicrometric pores. At the interface of similar or dissimilar metal pairs, such porosity occurs within an intermediate intermetallic phase. Interfaces of Al/Ti [8], Al/Steel [9–11], Al/Cu [12–15] and Al4000/Al7000 [16] in MPW are typical illustrative cases. Detailed observations at high magnification of these interfaces revealed a random distribution of the sub-micron pores within the intermediate intermetallic phase formed during the high-speed collision. The formation of such porous structure is attributed to a cavitation process of molten material in three stages including a nucleation, a growth and coalescence, and a solidification governed by the high-strain rate collision [17,18]. The nucleation and growth of pores may arise from a vaporization governed by a rapid isothermal and isochoric expansion of liquid metal due to a high rate of depressurization. A fast solidification at a high cooling rate of up to 10 °C/ns enables to freeze the micropores and to form the solidified porous architecture [17,18].

In the literature of impact welding, the characterization of the porous structure remains a subject of interest since such feature is an inherent structural property conferred by the impact mechanism itself. A few studies are available on this subject, and they mostly reveal the structure along with the shape and the size of the pores that are spherical and fine respectively, down to a few nanometres. In this paper, we investigate the mechanical feature of such porous structure and focus the analysis on the case of a porous $Al_xCu_y$ intermetallic produced at the interface of a tubular assembly (Al/Cu) welded by magnetic pulse welding.

## 2. Experimental methods

The welding was performed on a PULSAR MPW device using a discharge voltage of 8 kV and an initial air gap of 1.64 mm. Details of the welding conditions are available in our previous work which also provided the factual observation of intermediate $Al_xCu_y$ intermetallic pockets across the Al/Cu interface [7]. The governing mechanism for the formation of these pockets was also discussed in that previous work [7]. A high-resolution nanoindentation test on a polished surface of this pocket is used to map the local mechanical properties of the zone. Nanoindentation has been performed on a DCM II head of an Agilent G200 nanoindenter equipped with diamond Berkovich tip in CSM (continuous stiffness measurement) mode. The hardness distribution is characterized by a grid of 10x10 indents in an array fashion with a spacing of 6 ± 1 µm, an indentation strain rate of 0.05 $s^{-1}$ for a maximum depth of 250 nm. The hardness is calculated using the Oliver&Pharr model at depths in the range 180-200 nm. Prior to nanoindentation, the intermetallic pocket is observed by Scanning Electron Microscopy (SEM) and Energy Dispersive X-ray Spectroscopy (EDX) analysis to identify the composition of the $Al_xCu_y$ intermetallic and the porosity level in different zones.

## 3. Results and discussion

A representative $Al_xCu_y$ intermetallic pocket at the Al/Cu interface of the magnetic pulse weld of this study is shown on (Fig. 1). In our previous work, a temperature distribution was found near the zone of the intermetallic pocket (Fig. 2) suggesting that the alloying elements could have been heterogeneously distributed during the impact welding process. However, looking at the intermetallic pocket in the present paper, the measured alloying element distribution is found to be nearly homogeneous (Fig. 1) as more clearly evidenced by the individual measurements reported in (Table 1).

In contrast, the nanohardness distribution shows a strong gradient within the intermetallic $Al_xCu_y$ phase, and a lower value outside, i.e., within the parent metals. The intermetallic $Al_xCu_y$ phase exhibits a hardness in between 5-10 GPa (Fig. 3). These higher values compared to the values within both Al and Cu zones at the interface are expected to result from the nature of the $Al_xCu_y$ phase [13]. The hyper-quenching of the confined melted zone at the Al/Cu interface during the high-strain rate collision confers to the $Al_xCu_y$ liquid compound, a glass-like structure with high mechanical properties. The heterogenous hardness within the intermetallic $Al_xCu_y$ could have been interpreted as a result of heterogeneity in terms of $Al_xCu_y$ compound but the map of chemical compound characterized by EDX does clearly not lead to such a conclusion. The $Al_xCu_y$ intermetallic is an Al rich phase with a homogenous distribution of the Al compound (Table 1). On the diverse measured zones (zone 1 to 5), the content of Al is homogeneous enough to assume it is made of a unique $Al_xCu_y$ phase, expectedly $Al_2Cu$ (Table 1). This homogenous mixing is explained by the vortex kinematics that causes a local melting and involves a material mixing at the same time, as already discussed in our previous work [7].

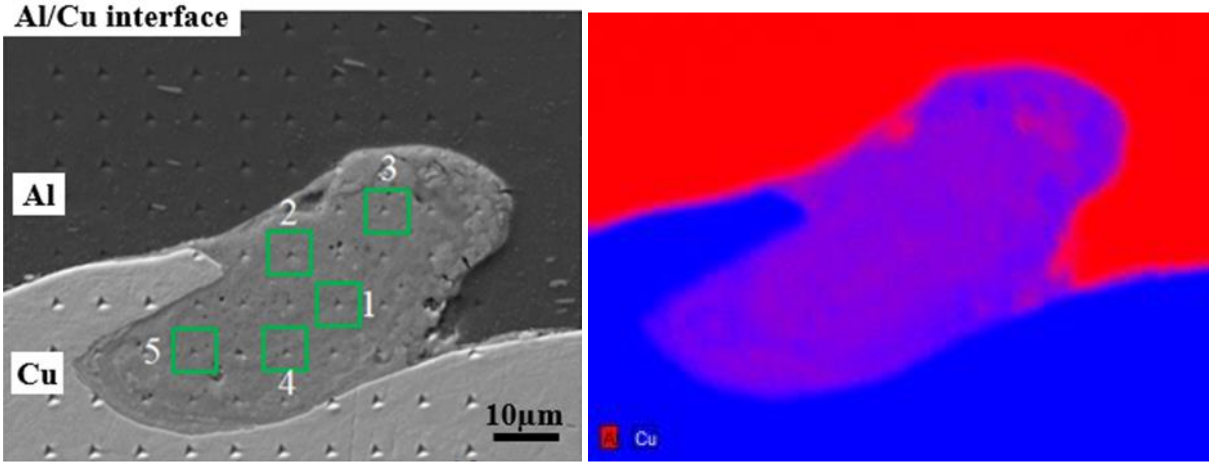


(a) (b)

Fig. 1. A high-resolution nanoindentation test on a polished surface across the Al/Cu interface containing a pocket of $Al_xCu_y$ intermetallic (a), and EDX scanning of the chemical content prior to the nanoindentation test (b). Values of Al and Cu atomic content on the zones 1 to 5 (denoted by the green square) are addressed in (Table 1).

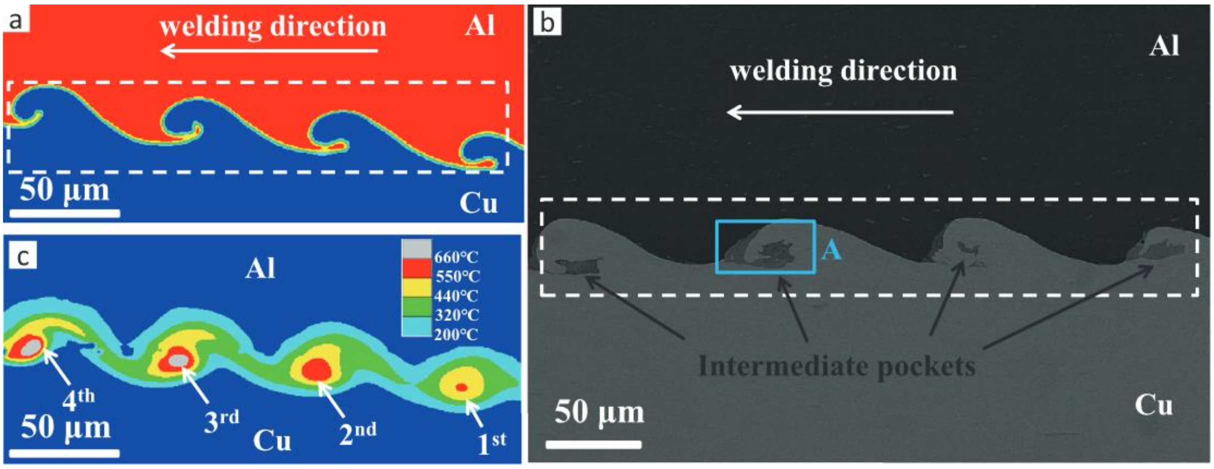


Fig. 2. Computational analysis of the impact process at the Al/Cu interface (a), compared to the experimental observation (b), and showing a thermal field surrounding the $Al_xCu_y$ intermetallic pocket (c), during the impact welding. Reproduced from [7] with the permission from Elsevier.

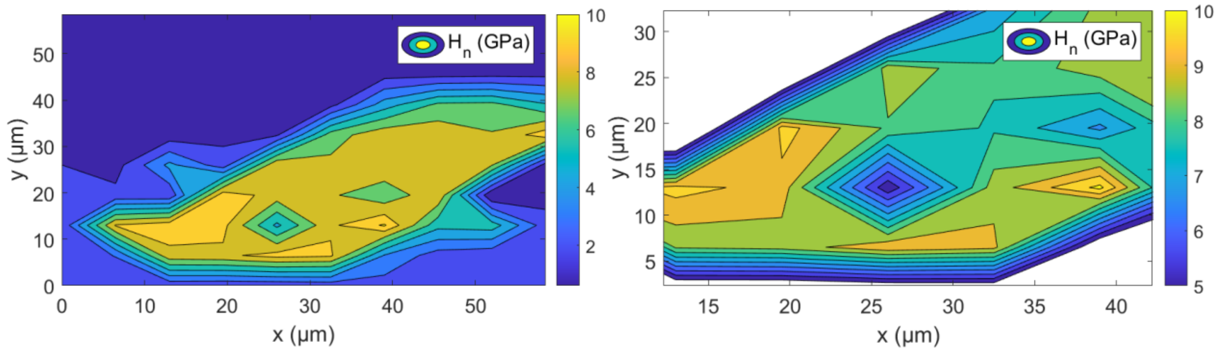

(a) (b)

Fig. 3. Hardness mapping of the intermetallic $Al_xCu_y$ phase by means of a high-resolution nanoindentation test showing a higher distribution and a heterogenous value within the intermetallic $Al_xCu_y$. Hardness range within the $Al_xCu_y$ phase and at both Al and Cu sides (a); hardness with a heterogenous distribution in the $Al_xCu_y$ phase over the range of 5-10 GPa (b). Nanoindentation using a grid of 10 x 10 indents in an array fashion with a spacing of 6±1 μm, an indentation strain rate of 0.05 $s^{-1}$ for a maximum depth of 250 nm.

Table 1. Chemical compound of the intermetallic $Al_xCu_y$ phase on disperse zones (zones 1 to 5 specified on Fig. 1a)

| Zone | 1 | 2 | 3 | 4 | 5 |
|---|---|---|---|---|---|
| Al (% at.) | 64.23 | 64.28 | 65.27 | 63.91 | 64.08 |
| Cu (% at.) | 35.77 | 35.52 | 34.73 | 36.09 | 35.92 |
| $H_n$ (GPa) | 5.10 | 6.85 | 7.93 | 8.75 | 9.72 |

The difference in hardness within the $Al_xCu_y$ intermetallic is rather a mechanical effect revealed by the comparison of the load-displacement (P-h) curves of the indented zones. The P-h curve of zone 5, corresponding to the curve with highest hardness, increases monotonously (Fig. 4a). The gradual decrease of hardness from one P-h curve to another is due pop-ins, i.e., a plateau of displacement during the loading of the indenter onto the intermetallic phase (Fig. 4b). From one P-h curve to another, the hardness decreases as the pop-in phenomenon becomes more prominent. Indeed, the plateau of displacement increases in number so that the P-h curves punctuated by recurrent pop-ins lead to a lowered hardness. Thereby, during the loading of the indenter, there is a cascade of critical forces that activates a sporadic plateau of displacement. The more pop-ins, the lower the hardness. The hardness drops from about 10 GPa to about 6 GPa while the ~10 GPa P-h curve does not exhibits prominent pop-ins such as those observed on the other P-h curves. The pop-in phenomenon appears on the ~9 GPa P-h curve and becomes more and more significant across the P-h curves of ~8 GPa, ~7 GPa and ~5 GPa. The link between the hardness decrease, the pop-in phenomenon, and the nature of intermetallic $Al_xCu_y$ itself can be related to the structure generated during the fast solidification of the $Al_xCu_y$ molten zone. Two major features characterize the $Al_xCu_y$ intermetallic phase due to the high-speed collision: an amorphous structure due to a hyper-quenching solidification as we already evidenced in our previous work [13], and also a nanoporous structure as characterized hereafter.

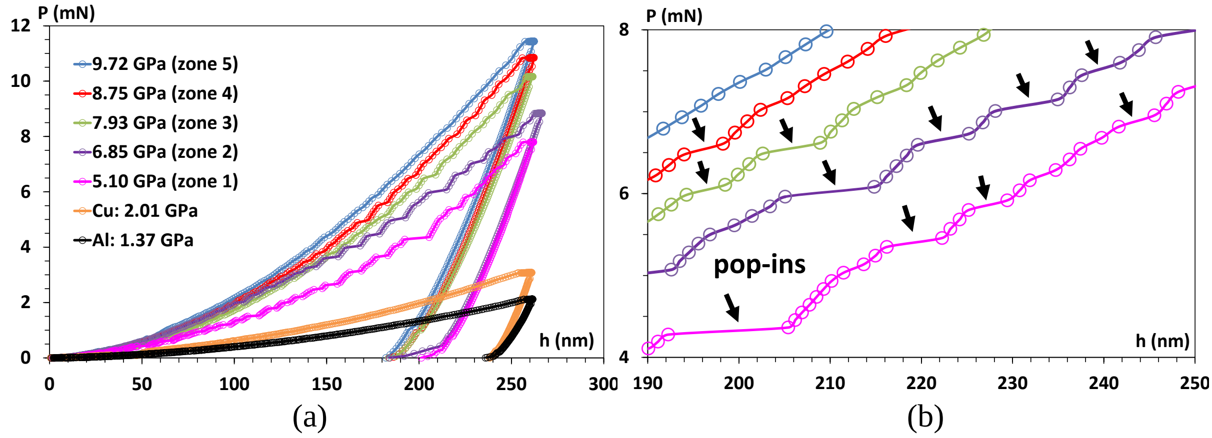


Fig. 4. Nanoindentation P-h curve and hardness within the intermetallic $Al_xCu_y$ and the parent metals. P-h responses (loading and unloading) of the diverse zones 1 to 5 (zones specified on Fig. 1a and indicated on Table 1) with the correspondence between the zone number and the hardness values given in (Table 1). High hardness P-h curve free of prominent pop-ins, and

occurrence of pop-ins on the P-h curves of lower hardness. Global view of each P-h curve (a) and magnified view on some pop-ins (b).

An amorphous metallic structure, known as bulk metallic glass, can produce a pop-in phenomenon during nanoindentation [19]. The pop-in response of the P-h curve has been correlated to the presence of serration at the periphery of the indenter. The serration appears as a cascading surface surrounding the indenter and each individual emerged surface has been interpreted as a result of localized shearing, denoted shear banding. The plateau of displacement is thus attributed to an unstable deformation due to bursts of highly localized strain that led to shear banding. The formation of shear bands is a reproductible phenomenon [20], and the shear band activity produces the pop-ins of the P-h curve [21]. In this paper, we rather rely on the porous structure of the intermetallic $Al_xCu_y$ media for discussing the decrease in hardness because the $Al_xCu_y$ phase was found to be nanoporous.

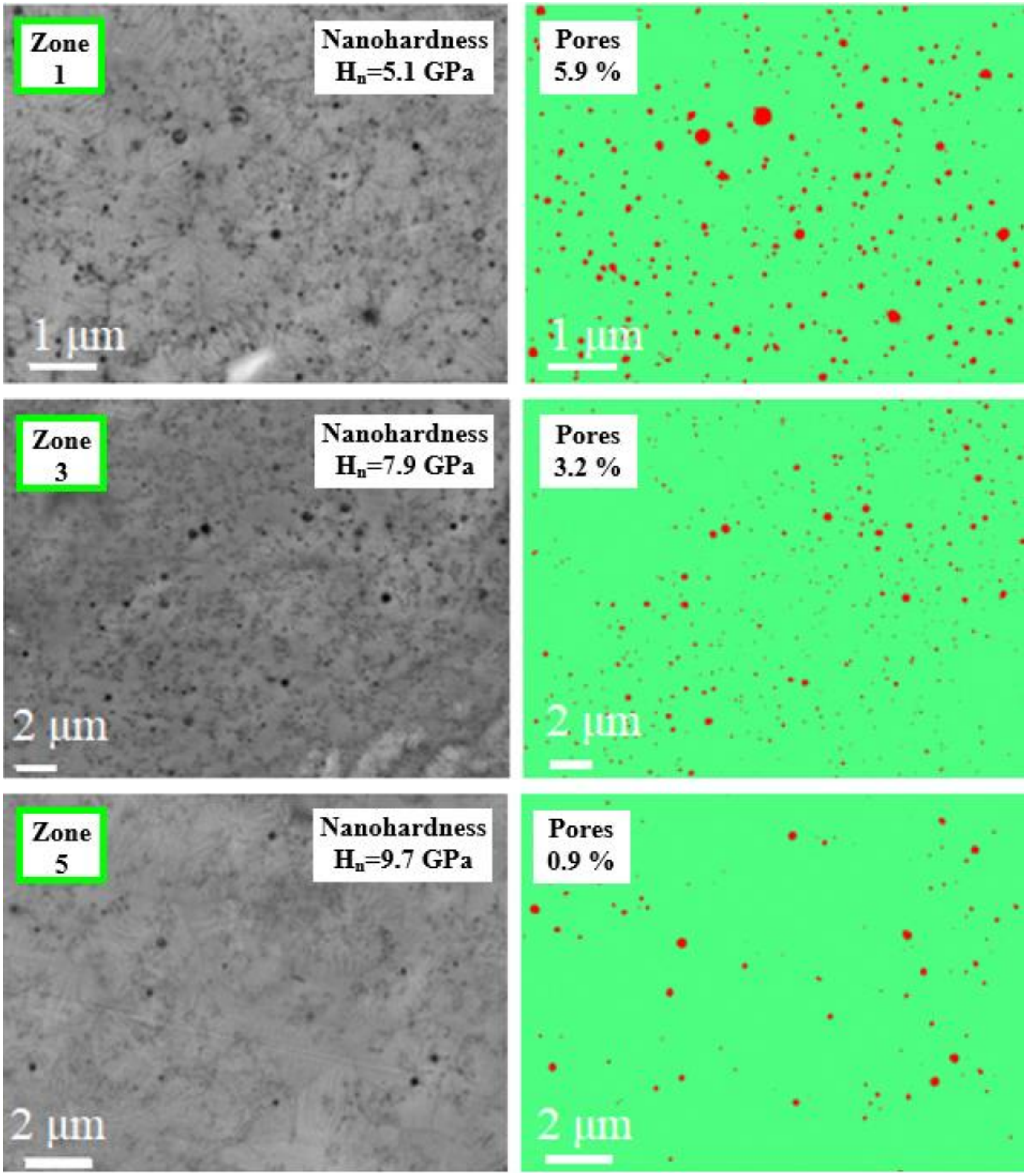


Fig. 5. Image analysis of the surface to be indented, to provide a characteristic porosity level of the intermetallic $Al_xCu_y$ phase in diverse zones (zone 1,3,5 specified on Fig. 1a) prior to nanoindentation. Nanohardness obtained in each zone: a very low porosity (0.9 %) for a very high nanohardness (9.7 GPa) that matches with the P-h curve free of prominent pop-ins (Fig. 4).

An analysis of pores fraction has been performed prior to nanoindentation. The nanopores fraction has been assessed from the surface observation of each sample, analysed using the ImageJ software. Typical results are illustrated in (Fig. 5). The porosity of the zones where these P-h curves were obtained has been correlated to the pop-ins features. The series of critical forces generated by the pop-ins are assessed from each curve of porosity fraction and then plotted depending on the indentation depth (Fig. 6). The comparison between the curves shows a relevant effect of the porosity fraction. There are two ranges: the range of low depths (below 60nm), and the range of larger depths (beyond 60nm). The range of shallow depths is magnified on (Fig. 6b). At the onset of the indentation (shallow depths), the level of critical forces is similar for the whole curves (Fig. 6b). However, the critical forces remain low for the case of lowest porosity fraction (0.9 %). The critical force does not exceed 1 mN (Fig. 6b). Such occurrence of limited critical force can be explained by a very limited pores interaction due the less content of pores. In case of higher pores fraction (2.8 %, 3.2 %, 4.6 %, 5.9%), the cascade of pop-ins is persistent. Then, there is still a series of critical forces. The comparison between the case of pores fraction of 2.8 %, 3.2 %, 4.6 % and 5.9 % shows that the critical force is lowered by a higher pores fraction (Fig. 6a). This result can be explained by a more probability of pores interactions because of a higher content of nanopores. As the indentation depth increases, the curve of highest porosity fraction exhibits the lowest values of critical force, as shown by the curve of 5.9 % pores fraction (Fig. 6a). Thereby, the critical loads are lowered by the porosity content. In addition, the total length of the plateaus increases with the porosity content (Fig. 7a). These observations correlate the nanopores to the pop-ins.

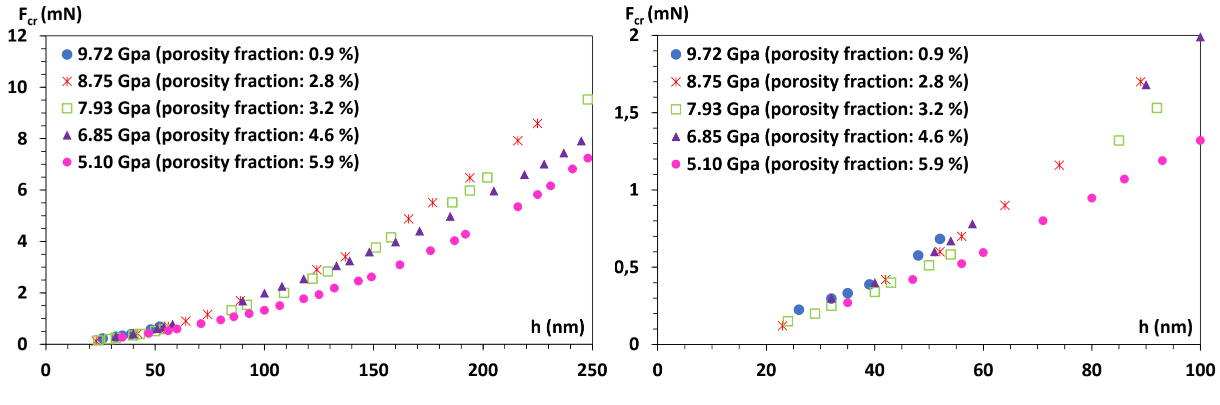


(a) (b)

Fig. 6. Critical force of pop-in plotted as a function of the indented depth, for each case of porosity fraction. Curves over the total indentation depth of 250 nm showing the effect of the pores content revealed at deep indentation (a), and curves at the onset of the indentation (short depths) showing very limited critical forces for the curve of lowest porosity fraction (b).

The pop-ins occurrence grows with the porosity fraction (Fig. 4), as also revealed by the cumulative length of plateaus (constant loading) generated by the pop-ins (Fig. 7a). The total cumulative length, denoted $L_P$, increases with the porosity fraction. This result shows a correlation between the pop-ins event and the porosity fraction. This correlation is in accordance with the hardness of the nanoporous zones which decreases with the increase of porosity fraction (Fig. 7b). The fact that the pop-in leads to a hardness decrease further supports the mechanism of pores interaction due to the nanoporosity. The P-h curve of highest hardness (~10 GPa) corresponds to a low porosity (0.9 %). The prominence of the pop-ins on the P-h curve of lowest hardness (~5 GPa) is also a relevant indication of pore content effect. Thereby, because of a higher porosity fraction, there is a more probability of interactions between the nanopores due to the stress concentration that can ease a mechanism of cracks formation and propagation, and thus, a sudden displacement characterizing a pop-in response on the P-h curve. Thereby, the formation of nanopores during the high-strain rate collision can degrade the mechanical performance of the $Al_xCu_y$ intermetallic media. For the case in this paper, the hardness is halved (Fig. 4). Minimizing the porosity enables an improvement of the weld quality but the high strain rate collision with its random process is difficult to control. Together, these observations evidence how the porous nature of the intermetallic $Al_xCu_y$ phase can decrease the mechanical property of the Al/Cu weld.

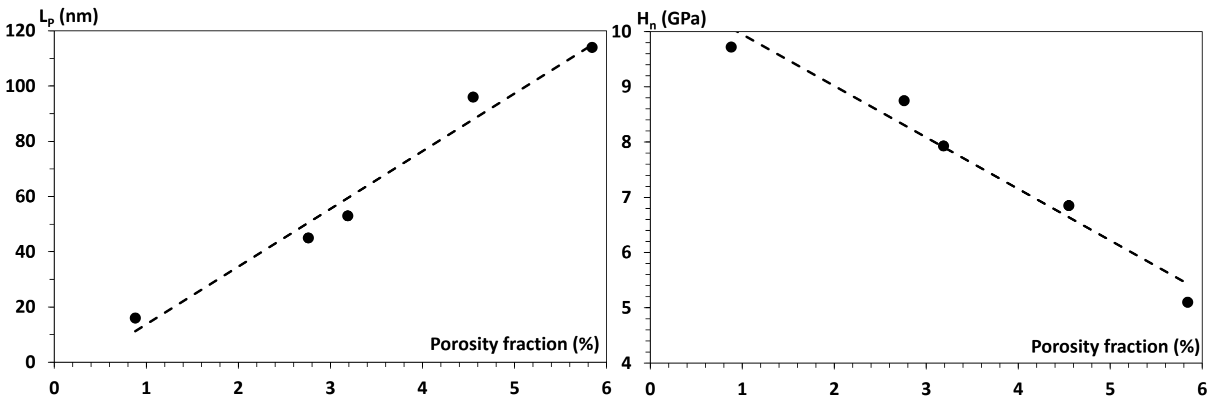


(a) (b)

Fig. 7. Correlation of the porosity fraction to the pop-ins event of the nanoporous $Al_xCu_y$ intermetallic phase. Total cumulative length of plateaus generated the pop-ins, denoted $L_P$, plotted as a function of the porosity fraction (a). Hardness depending on the porosity fraction that further correlates the pop-in event of the P-h curve to the porosity fraction (b).

## 4. Conclusions

Impact welding of dissimilar metal pairs generally involves the formation of an intermetallic phase at the welded interface during the high-speed collision. In this paper, we focused on the characterization of such phase at the Al/Cu interface produced by magnetic pulse welding. The $Al_xCu_y$ intermetallic phase consists of a $Al_2Cu$ compound with a nanoporous structure. The hardness of the intermetallic $Al_2Cu$ phase ranges in between 5-10 GPa, whereas the base metal exhibits a lower hardness of about 1.4 GPa on the Al side, and of about 2 GPa on the

Cu side. The high-resolution nanoindentation within the *$Al_2Cu$* phase shows a P-h curve with pop-ins phenomenon that causes a gradual decrease of the hardness. This observation suggested an occurrence of a cascade of critical forces beneath the indent that activates a sporadic plateau of displacement. With the interpretation of the hardness decrease, the pop-in phenomenon was related to the nanoporous structure of the *$Al_2Cu$* phase. As the nanopores fraction increases from ~1 % to ~6 %, the hardness decreases twofold (from about 10 GPa to about 5 GPa) with a linear tendency. The total length of plateaus produced by the pop-ins increases with the nanopores fraction following a linear tendency also. The critical force of pop-ins is lowered by the porosity content. The curve of highest porosity fraction exhibits the lowest values of critical force. These observations correlate the nanopores to the pop-ins.

**References**


[1] H. Wang, Y. Wang, High-Velocity Impact Welding Process: A Review, Metals. 9 (2019) 144. https://doi.org/10.3390/met9020144.

[2] J. Lueg-Althoff, J. Bellmann, S. Gies, S. Schulze, A.E. Tekkaya, E. Beyer, Influence of the flyer kinetics on magnetic pulse welding of tubes, Journal of Materials Processing Technology. 262 (2018) 189–203. https://doi.org/10.1016/j.jmatprotec.2018.06.005.

[3] A. Kapil, A. Sharma, Magnetic pulse welding: an efficient and environmentally friendly multi-material joining technique, Journal of Cleaner Production. 100 (2015) 35–58. https://doi.org/10.1016/j.jclepro.2015.03.042.

[4] Y. Zhang, S.S. Babu, C. Prothe, M. Blakely, J. Kwasegroch, M. LaHa, G.S. Daehn, Application of high velocity impact welding at varied different length scales, Journal of Materials Processing Technology. 211 (2011) 944–952. https://doi.org/10.1016/j.jmatprotec.2010.01.001.

[5] A. Vivek, S.R. Hansen, B.C. Liu, G.S. Daehn, Vaporizing foil actuator: A tool for collision welding, Journal of Materials Processing Technology. 213 (2013) 2304–2311. https://doi.org/10.1016/j.jmatprotec.2013.07.006.

[6] R.N. Raoelison, T. Sapanathan, E. Padayodi, N. Buiron, M. Rachik, Interfacial kinematics and governing mechanisms under the influence of high strain rate impact conditions: Numerical computations of experimental observations, Journal of the Mechanics and Physics of Solids. 96 (2016) 147–161. https://doi.org/10.1016/j.jmps.2016.07.014.

[7] J.S. Li, R.N. Raoelison, T. Sapanathan, Y.L. Hou, M. Rachik, Interface evolution during magnetic pulse welding under extremely high strain rate collision: mechanisms, thermomechanical kinetics and consequences, Acta Materialia. 195 (2020) 404–415. https://doi.org/10.1016/j.actamat.2020.05.028.

[8] H. Wang, K. Wang, W. Zheng, Microstructure complexities of laser impact welded Al-Ti bonding interface, Scripta Materialia. 211 (2022) 114488. https://doi.org/10.1016/j.scriptamat.2021.114488.
[9] P. Wang, D. Chen, Y. Yan, X. She, B. Feng, Y. Ran, H. Peng, D. Li, X. Jiang, Hierarchical Morphology and Formation Mechanism of Collision Surface of Al/Steel Dissimilar Lap Joints via Electromagnetic Pulse Welding, Metals. 11 (2021) 1468. https://doi.org/10.3390/met11091468.
[10] H. Yu, Z. Xu, Z. Fan, Z. Zhao, C. Li, Mechanical property and microstructure of aluminum alloy-steel tubes joint by magnetic pulse welding, Materials Science and Engineering: A. 561 (2013) 259–265. https://doi.org/10.1016/j.msea.2012.11.015.
[11] L. Zhang, J. Wen, Y. Chen, L. Yin, J. Xie, D. Xiong, H. Zhang, W. Zhang, L. Zhang, Interfacial defects evolution of Al 6061 / SS304 electromagnetic pulse welding joints during post welding isothermal treatment, Materials Today Communications. 35 (2023) 106295. https://doi.org/10.1016/j.mtcomm.2023.106295.
[12] R.N. Raoelison, T. Sapanathan, N. Buiron, M. Rachik, Magnetic pulse welding of Al/Al and Al/Cu metal pairs: Consequences of the dissimilar combination on the interfacial behavior during the welding process, Journal of Manufacturing Processes. 20 (2015) 112–127. https://doi.org/10.1016/j.jmapro.2015.09.003.
[13] R.N. Raoelison, D. Racine, Z. Zhang, N. Buiron, D. Marceau, M. Rachik, Magnetic pulse welding: Interface of Al/Cu joint and investigation of intermetallic formation effect on the weld features, Journal of Manufacturing Processes. 16 (2014) 427–434. https://doi.org/10.1016/j.jmapro.2014.05.002.
[14] J.S. Li, T. Sapanathan, R.N. Raoelison, Y.L. Hou, A. Simar, M. Rachik, On the complete interface development of Al/Cu magnetic pulse welding via experimental characterizations and multiphysics numerical simulations, Journal of Materials Processing Technology. (2021) 117185. https://doi.org/10.1016/j.jmatprotec.2021.117185.
[15] G. Göbel, J. Kaspar, T. Herrmannsdörfer, B. Brenner, Insights into intermetallic phases on pulse welded dissimilar metal joints, (2010) 10.
[16] M. Pourabbas, A. Abdollah-zadeh, M. Sarvari, M. Pouranvari, R. Miresmaeili, Investigation of structural and mechanical properties of magnetic pulse welded dissimilar aluminum alloys, Journal of Manufacturing Processes. 37 (2019) 292–304. https://doi.org/10.1016/j.jmapro.2018.12.002.
[17] T. Sapanathan, R.N. Raoelison, N. Buiron, M. Rachik, In situ metallic porous structure formation due to ultra high heating and cooling rates during an electromagnetic pulse welding, Scripta Materialia. 128 (2017) 10–13. https://doi.org/10.1016/j.scriptamat.2016.09.030.
[18] R.N. Raoelison, J. Li, T. Sapanathan, E. Padayodi, N. Buiron, D. Racine, Z. Zhang, D. Marceau, M. Rachik, A new nature of microporous architecture with hierarchical porosity and membrane template via high strain rate collision, Materialia. 5 (2019) 100205. https://doi.org/10.1016/j.mtla.2018.100205.
[19] C.A. Schuh, T.G. Nieh, A nanoindentation study of serrated flow in bulk metallic glasses, Acta Materialia. 51 (2003) 87–99. https://doi.org/10.1016/S1359-6454(02)00303-8.
[20] W.H. Jiang, M. Atzmon, Rate dependence of serrated flow in a metallic glass, Journal of Materials Research. 18 (2003) 755–757. https://doi.org/10.1557/JMR.2003.0103.
[21] B. Moser, J. Kuebler, H. Meinhard, W. Muster, J. Michler, Observation of Instabilities during Plastic Deformation by in-situ SEM Indentation Experiments, Advanced Engineering Materials. 7 (2005) 388–392. https://doi.org/10.1002/adem.200500049.